9-30-2019

Proton Transfer versus Hydrogen Bonding in a Reduced Iron Porphyrin Nitrosyl Complex

Md. Hafizur Rahman
Marquette University

Yilin Liu
Marquette University

Michael D. Ryan
Marquette University, michael.ryan@marquette.edu

Inorganic Chemistry, Vol. 58, No. 20 (2019) : 13788-13795. DOI.

Proton Transfer versus Hydrogen Bonding in a Reduced Iron Porphyrin Nitrosyl Complex

Md. Hafizur Rahman
Chemistry Department, Marquette University, Milwaukee, Wisconsin
Yilin Liu
Chemistry Department, Marquette University, Milwaukee, Wisconsin
Michael D. Ryan
Chemistry Department, Marquette University, Milwaukee, Wisconsin

Abstract

The ^{1}H NMR spectra of Fe(OEP)(HNO), which was formed from Fe(OEP)(NO)$^{-}$ in the presence of 3,5-dichlorophenol, were studied as a function of temperature. The chemical shift of the HNO proton showed a unique behavior which could be explained based on the equilibrium between the protonated complex, Fe(OEP)(HNO), and the hydrogen-bonded complex, Fe(OEP)(NO)$^{-}$···HOPh. This equilibrium was consistent with UV/visible spectroscopy and the voltammetric data. UV/visible stopped-flow experiments showed that the hydrogen-bonded complex, which was formed when weak acids such as phenol were added, and the Fe(OEP)(HNO) complex were quite similar. In addition to the HNO proton resonance, the *meso*-resonances were consistent with the proposed equilibrium. Density functional theory calculations of various Fe(OEP)(NO)$^{-}$/Fe(OEP)(HNO) species were calculated, and the results were consistent with experimental data.

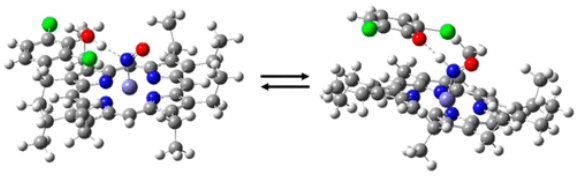

Synopsis

Using ^{1}H NMR spectra, the equilibrium between Fe(OEP)(HNO) and Fe(OEP)(NO)$^{-}$ hydrogen bonded to phenol was studied as a function of temperature. Voltammetric data, visible spectroscopy, and DFT calculations were used to study this equilibrium.

Introduction

The formation of HNO complexes has been the focus of considerable research in recent years.(1−7) The HNO moiety has been implicated in a number of enzymes including cytochrome *c* nitrite reductase,(8,9) fungal P450 nitric oxide reductase,(10,11) and hydroxylamine oxidoreductase.(12) The pharmacology and therapeutic potential of HNO has been reviewed by Paolocci et al.(13) and Miranda.(14) The synthesis of a Fe(P)(HNO) complex, where P = porphyrin, was first reported by Lin and Farmer(15) for an HNO complex with myoglobin. Farmer et al.(16−18) further studied the complex with NMR, X-ray absorption, and resonance Raman spectroscopies. Farmer and Sulc(19) reviewed the coordination chemistry of HNO and hemes. The Fe(OEP)(HNO)(MeIm) complex (MeIm = methylimidazole) was synthesized by Abucayon et al.(2) using a hydride attack on a ferric nitrosyl porphyrin. Using density functional theory (DFT) calculations, they traced the N-pathway addition of hydride to the ferric nitrosyl.(2) Abucayon et al.(20) showed that, under some conditions, the hydride ion can bond directly to the iron, rather than the nitrogen. Rahman and Ryan(6) generated an Fe(OEP)(HNO) complex by reaction of a {Fe(NO)}^{8} porphyrin complex with substituted phenols. The acidity and hydrogen exchange dynamics of a nonheme Fe^{II}(HNO) complex was studied by Gao et al.(21) using NMR. They determined that the pK_a value for that HNO complex to be greater than 11, confirming that the {Fe(HNO)}^{8} complex had a high pK_a.(22,23) Recently, Levin et al.(24) found remarkable changes in the acidity of a nonheme {Fe(HNO)}^{8} as the structure of the iron ligand was changed.

The DFT structures and infrared and NMR spectra of 5- and 6-coordinate {Fe(HNO)}^{8} porphyrin complexes were reported.(2,3,6,20,25) In general, all the structures predicted a resonance for the HNO proton around 13–14 ppm. DFT calculations showed that protonation of the anion was most favorable on the nitrogen atom.(26) For the five-coordinate Fe(OEP)(NO)$^{-}$ complex, the *meso*-protons were upshifted from their normal diamagnetic positions between 10 and 11 ppm because of the displacement of the iron from the porphyrin plane.(6)

As discussed above, the {Fe(HNO)}8 complex can be generated by either the hydride reduction of the ferric nitrosyl complex or the protonation of the {Fe(NO)}8 complex (a Brønsted acid/base reaction). Reactions of Brønsted acids with Brønsted bases in water generally lead to ionic products if the equilibrium is favorable:

$$\mathrm{AH} + \mathrm{B} \rightleftarrows \mathrm{A}^{-} + \mathrm{HB}^{+} \quad (1)$$

In aprotic solvents, the reaction is more complex.(27) Ionization might not occur, and the resulting complex is a hydrogen-bonded complex:

$$\mathrm{AH} + \mathrm{B} \rightleftarrows \mathrm{AH} \cdots \mathrm{B} \quad (2)$$

These products correspond to two wells on the potential energy surface where the proton is covalently bonded to either A or B.(28) In most cases, either the ionic product or the hydrogen-bonded complex will dominate. An equilibrium therefore exists between the two products:

$$\mathrm{AH\cdots B \rightleftarrows A^- + HB^+}\ (3)$$

The equilibrium between these two species is certainly temperature-dependent, and the dominant species in solution will change as a function of temperature. An example of this was the reaction of acetic acid with trimethyl amine in an aprotic solvent. This reaction was studied using ^{1}H NMR.(29) By varying the temperature, they were able to shift the position of the equilibrium for reaction 3. Golubev et al. used NMR to study the shift from an O···H–N species to an O–H···N species as a function of temperature in an intramolecular charge relay chain in a model Schiff base.(30) This problem was studied by Zundel(28) using theoretical calculations and infrared spectroscopy. In the gas phase, the hydrogen-bonded species will dominate. With the addition of solvent interactions, the equilibrium position can shift toward the ionic product.

Voltammetric and spectroelectrochemical studies have been carried out for the reduction of Fe(OEP)(NO) in the presence of weak acids. Cyclic voltammetry and rotating ring disk electrode (RRDE) voltammetry showed that the reduction wave for Fe(OEP)(NO) to the anion was shifted to more positive potentials with the addition of 2,6-dichlorophenol (2,6-dcp).(31) This was consistent with the following reaction:

$$\mathrm{Fe(OEP)(NO) + e^- \rightleftarrows Fe(OEP)(NO)^-}\ (4)$$

$$\mathrm{Fe(OEP)(NO)^- + PhOH \rightleftarrows Fe(OEP)(HNO) + PhO^-}\ (5)$$

The variation of the collection efficiency with rotation rate showed that reaction 5 was chemically reversible and that the reverse process for that reaction was slow. In addition, it was shown that H_2 was not generated voltammetrically by the reaction of Fe(OEP)(NO)$^-$/phenol under these conditions.(31)

Infrared spectroelectrochemistry of Fe(OEP)(NO) has been carried out in our laboratory.(6,32) The ν_{NO} bands for Fe(OEP)(NO) and Fe(OEP)(NO)$^-$ were observed in the infrared spectra, but no $^{14/15}$N-isotope sensitive bands could be observed for Fe(OEP)(HNO), probably because of weak absorbance of the bands and/or overlap with porphyrin-related vibrations in the mid-infrared region.(6,32) Attempts to observe the ν_{HNO} band using $^{1/2}$H-isotope substitution also failed because of spectral overlap, which was confirmed by DFT calculations.(32) For the more reduced complex (Fe(OEP)(H_2NOH)), the ν_{H-N} bands were observed and were confirmed by $^{1/2}$H-isotope substitution.(32) Some success was obtained using resonance Raman spectroscopy. In the low-frequency region, the ν_{FeNO} band for Fe-HNO myoglobin were observed by Immoos et al.(17) and Czanecki and Kincaid,(33) though their absorbances were weak and subject to overlap. In the midfrequency region, Immoos et al.(17) used spectral simulation of the region around the strong 1374 cm^{-1} porphyrin bond to find a very weak band which was assigned to the ν_{NO} vibration of Fe-HNO myoglobin. Only the ^{15}N substituted band was observed. Because of the difficulties of using vibrational spectroscopy, we turned to ^{1}H NMR spectroscopy where it was possible to directly observe the proton on the Fe-HNO moiety of the {Fe(HNO)}^{8} porphyrin complex.

The formation of Fe(OEP)(H^{15}NO) using an acid/base reaction between the {Fe(NO)}^{8} complex and 2,6-dcp gave a resonance for the proton in the HNO group at 12.6 ppm.(6) This was similar to the resonance observed earlier for a six-coordinate Fe(OEP)(HNO) complex.(2) Using an NOE experiment, it was shown that the HNO proton at 12.60 ppm was in exchange with the free phenol species.(6) As a result, no splitting of the H^{15}NO proton was observed. In order to slow down the exchange, a temperature study was carried out, and the results will be presented below. The behavior of the HNO proton as a function of temperature was unusual and can be explained by reaction 3. The shift in equilibrium between a protonated and hydrogen-bonded complex has significant consequences for spectroscopic experiments that are carried out at low temperatures. The identity of the species may change as the temperature is reduced from ambient temperatures.

Experimental Section

Chemicals

Tetrabutylammonium perchlorate (TBAP), iron(III) octaethylporphyrin (FeOEPCl), 3,5-dichlorophenol (3,5-dcp), 2,6-dichlorophenol (2,6-dcp), sodium methoxide, and hydroxylamine hydrochloride were purchased from Sigma-Aldrich Chemical Co. Deuterated phenols (phenol-d_5, 3,5-dichlorophenol-d_3, and 3,5-dichlorophenol-d_4) were obtained from CDN Isotopes. Tetrabutylammonium perchlorate (TBAP) was dried at 90 °C under a vacuum overnight before use. Anhydrous tetrahydrofuran (THF) was refluxed in the presence of sodium metal and benzophenone until the solution was a persistent dark blue color. After purification, the solvent was collected under argon and stored in a glovebox. All phenols were purified by sublimation. The Fe(OEP)(NO) and Fe(OEP)$(NO)^-$ complexes and their ^{15}NO adducts were synthesized by literature methods.(34−36)

Instrumentation

The UV–visible spectra were recorded on an HP 8452A diode array spectrophotometer. NMR measurements were performed using a Varian 400 MHz FT spectrometer. Rotating ring-disk electrode (RRDE) experiments were carried out as previously described.(31) Stopped-flow experiments were performed by Olis RSM 100 SF from Bogart, GA. All resonance Raman spectra were acquired with the 406.7 nm excitation line from a Kr^+ laser (Coherent Innova Sabre Ion Laser). A Spex 1269 spectrometer equipped with a Spec-10 LN-cooled detector having 2048 pixels (Princeton Instruments, NJ) was used. The laser power was kept at ∼1 mW, and the NMR sample tubes were spun to avoid laser-induced heating and photodissociation. Measurements at 77 K were done by immersing the tube in a double-walled quartz cell which was filled with liquid nitrogen. Each spectrum was collected in 10 min increments, over a 2 h period. The spectra were then averaged. The slit width was set at 150 μm, and the 1200 g/mm grating were used. Spectra were calibrated with fenchone (Sigma-Aldrich, WI) and processed with Grams/32 AI software (Galactic Industries, Salem, NH).

Procedures

All solutions were prepared in the glovebox and sealed with Teflon tape. The argon gas flow was continued above the voltammetric solutions until the end of the experiment. The argon gas was presaturated with THF for the voltammetric experiments. For the stopped-flow experiments, one solution contained the acid to be studied in THF while the second solution contained Fe(OEP)$(NO)^-$, which was chemically reduced as described previously.(6) Both solutions were prepared in the glovebox and transferred to the stopped-flow instrument via gastight syringes. The DFT calculations for the NMR and vibrational spectra were calculated using the procedures described previously.(34)

Results and Discussion

^1H NMR Spectroscopy

The ^1H NMR spectrum of 3,5-dichlorophenol-d_3 with Fe(OEP)$(^{15}NO)^-$ is shown in Figure 1. The phenyl deuterated 3,5-dichlorophenol-d_3 was used in order to minimize the signal for the phenyl protons which would dominate the NMR signal as it was in excess. This made it easier to observe the signals for the Fe(OEP)$(H^{15}NO)$ complex. At 20°, a proton resonance at 12.60 ppm was observed. The strong resonance between 9 and 10 ppm is due to the excess of 3,5-dichlorophenol-d_3. The temperature was then decreased in 20° increments. The initial aim of this work was to slow the proton exchange which had prevented us from seeing the $^1H–^{15}N$ splitting. The results are shown in Figure 1. If the resonance at 12.60 ppm (20 °C) was due to slow exchange between free phenol and the proton on the Fe-HNO moiety, the two resonances should have moved apart as the temperature was lowered and the exchange reaction was slowed down. Instead, the resonance for the hydrogen atom on the HNO moiety moved upfield as the temperature was decreased, and the shift in the resonances was reversible (Figure 1 and Table S1). As the temperature increased, the resonances occurred at the same values as were

observed in the cooling cycle. In addition, at each temperature, the resonances were independent of time, further confirming that the shift was not due to an irreversible reaction. ^{2}H NMR of Fe(OEP)(^{15}NO)$^{-}$ with 3,5-dcp-d_4 was carried out in THF at −40 °C (Figure S1). A resonance was observed very similar to the proton spectrum with a chemical shift of 11.10 ppm vs TMS (the small difference between the ^{1}H and ^{2}H spectra was probably due to isotopic effects on the equilibria discussed below).

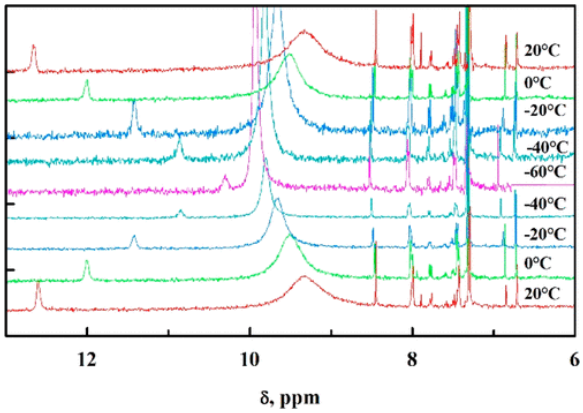

Figure 1. ^{1}H NMR spectra of chemically generated 8 mM Fe(OEP)(^{15}NO)$^{-}$ with 10 mM 3,5-dcp-d_3 in THF-d_8. Increasing time from bottom to top.

The best explanation for this behavior is a fast exchange between the protonated and unprotonated {Fe(NO)}^{8} species. Previous studies have indicated that the room-temperature species is the Fe(OEP)(HNO) complex. Two other {Fe(NO)}^{8} species can be formed as the temperature was decreased: Fe(OEP)(NO)$^{-}$ or Fe(OEP)(NO)$^{-}$···HOPh (hydrogen-bonded complex, 1). The first complex is consistent with reaction 1, while the second complex follows reaction 2. Further verification for the shift in equilibrium with temperature can be seen in the 8–10 ppm region. The spectra for 20 and −60 °C are shown in Figure 2, expanding the *x*-axis to focus on the region where the *meso*-protons are observed. The spectrum at 20 °C was consistent with the Fe(OEP)(^{15}HNO) complex that has been previously reported.(6) As the temperature was decreased, new resonances were observed at 7.68, 7.51, and 7.43 ppm at −60 °C, indicating that a new chemical species was present at this temperature. When 3,5-dcp-d_3 was replaced with phenol-d_5, the resonance for the proton in the HNO moiety was not observed, and the *meso*-resonances observed with 3,5-dcp-d_3 at 20 °C were not observed, indicating that phenol did not form a Fe(OEP)(HNO) complex.

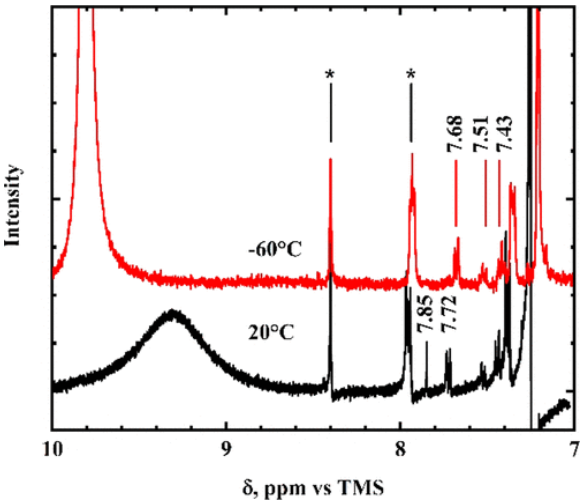

Figure 2. ^{1}H NMR spectra of 8 mM Fe(OEP)(^{15}NO)$^{-}$ in the presence of 10 mM 3,5-dcp-d_3 in THF-d_8. Black trace: 20 °C. (*) indicates anthracene bands from the reducing agent. Red trace: −60 °C.

These results are consistent with an equilibrium between $Fe(OEP)(NO)^-$ (with or without hydrogen bonding to phenol) and the Fe(OEP)(HNO) complex, as described by reaction 1 or 2. The observed resonance in the 10–13 ppm region is the average of two species: the Fe(OEP)(HNO) (δ_{HNO}) and the $Fe(OEP)(NO)^-$ or the hydrogen-bonded complex (δ_{NO}).(29) The observed position is dependent on the concentration of each species, as given by

$$\delta = \delta_{NO}\left(\frac{1}{1+K}\right) + \delta_{HNO}\left(\frac{K}{1+K}\right) \quad (6)$$

Fast exchange gives rise to a single resonance for the two species. If $Fe(OEP)(NO)^-$ is hydrogen-bonded, one would expect exchange between that species and free phenol, which will probably exchange faster than the Fe(OEP)(HNO)-phenol exchange (giving rise to a three way exchange between phenol, Fe(OEP)(HNO), and $Fe(OEP)(NO)^-$/hydrogen bond).

As the temperature is reduced, the dominant species became an $Fe(OEP)(^{15}NO)^-$ complex. If that complex is a hydrogen-bonded complex, there would still be no $^1H–^{15}N$ splitting.(30) Therefore, at room temperature, no splitting was observed because of the exchange reaction, and at low temperatures, the dominant species (free $Fe(OEP)(NO)^-$ with or without hydrogen bonding) would not generate any $^1H–^{15}N$ splitting.(30,37)

Voltammetry of Fe(OEP)(NO) in 3,5-Dichlorophenol/THF and Visible Spectroscopy

The voltammetry of Fe(OEP)(NO) in the absence and presence of 10 mM 3,5-dcp is shown in Figure 3. The potential shifts followed the Nernst equation, and in the presence of 10 mM 3,5-dcp, the reduction wave was shifted by 52 mV where PhOH = 3,5-dcp. The results follow the mechanism given by reactions 4 and 5. In addition to the potential shift, the collection efficiency ($N_k = -i_R/i_D$) also decreased from the chemically reversible value. This indicated that the oxidation of Fe(OEP)(HNO) to Fe(OEP)(NO) was slow on the RRDE time scale. The shift of 52 mV was consistent with the formation of at least 95% Fe(OEP)(HNO). This would indicate that the Fe(OEP)(HNO) complex was the dominate species in solution at room temperature. Weaker acids such as phenol (pK_a = 10.0 versus 8.18 for 3,5-dcp) showed no shift in the $E_{1/2}$ value unless high concentrations of phenol were added (greater than 0.10 M for phenol) (Figure S2). For example, the $E_{1/2}$ value for Fe(OEP)(NO) reduction was unchanged with the addition of 50 mM phenol (no phenol, −1.456 V; 50 mM phenol, −1.458 V). The collection efficiencies were also unchanged, consistent with the ^1H NMR spectrum that showed that Fe(OEP)(HNO) was not formed under these conditions.

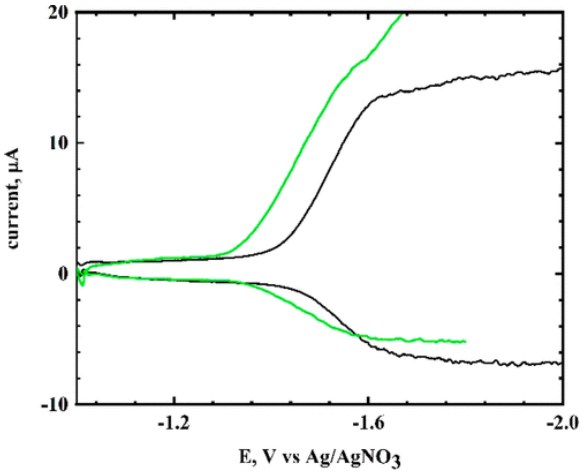

Figure 3. Rotating ring-disk voltammetry of 0.45 mM Fe(OEP)(NO) in THF in the absence (black) and presence of 10 mM 3,5-dichlorophenol (green). Ring and disk electrode: platinum. Electrolyte: 0.10 M TBAP. Rotation rate: 50 rpm.

Given the ^1H NMR spectra, the $\{Fe(NO)\}^8$ species at lower temperatures is different from the room-temperature species. If this low-temperature species has a visible spectrum different from the room-temperature species,

there should be a change in the visible spectra. The visible spectra of Fe(OEP)(NO)$^-$ in 3,5-dcp/THF at two different temperatures are shown in Figure 4 (red and blue traces), along with the spectrum for Fe(OEP)(NO)$^-$ without 3,5-dcp (black trace). The spectra of Fe(OEP)(NO)$^-$ and Fe(OEP)(HNO) are quite different so that mixtures of these species should be observed. Reduction of the temperature to −18 °C (Figure 4, blue trace) caused only minor changes in the visible spectrum, even though the ^{1}H NMR spectra showed a significant decrease in the concentration of the Fe(OEP)(HNO) species. This indicated that the iron porphyrin species formed at low temperatures was not Fe(OEP)(NO)$^-$. On the basis of the visible and ^{1}H NMR spectra, the most likely species was a hydrogen-bonded Fe(OEP)(NO)$^-$ species.

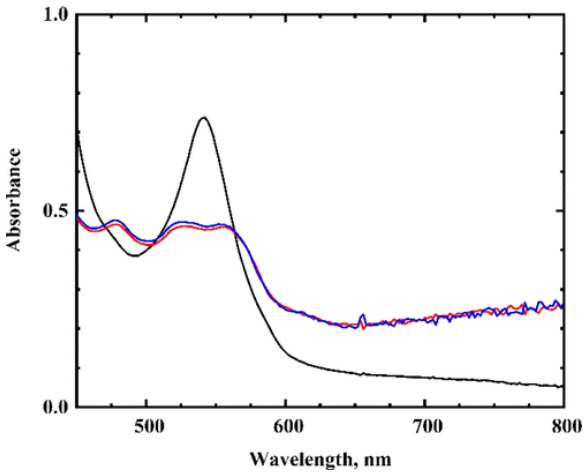

Figure 4. Visible spectra of 0.29 mM Fe(OEP)(NO)$^-$ in THF with 3,5-dichlorophenol-d_3 at 12 °C (red) and −18 °C (blue). Black trace: Fe(OEP)(NO)$^-$ without 3,5-dichlorophenol-d_3.

In order to further characterize the hydrogen-bonded {Fe(NO)}^{8} species, stopped-flow experiments were carried out with chemically generated Fe(OEP)(NO)$^-$ and phenols. Several phenolic species were studied, and the visible spectra for the mixtures of Fe(OEP)(NO)$^-$/phenol were quite similar. The spectra for the reaction of Fe(OEP)(NO)$^-$ with 2,6-dcp (strongest acid studied) (Figure S3), which is known to form Fe(OEP)(HNO), showed a spectrum very similar to that observed in Figure 4 (traces red and blue). Voltammetry and ^{1}H NMR spectroscopy indicated that Fe(OEP)(HNO) was formed with 2,6-dcp under the conditions of the stopped-flow experiment.(6,31) Phenol itself (weakest acid studied), when reacted with Fe(OEP)(NO)$^-$, gave a spectrum similar to Fe(OEP)(HNO) from the reaction with 2,6-dcp (Figure 5, black and red traces). Voltammetric data have shown that Fe(OEP)(HNO) was not formed at these concentrations of phenol. These results confirm that Fe(OEP)(HNO) and the hydrogen-bonded complex of Fe(OEP)(NO)$^-$ have similar visible spectra.

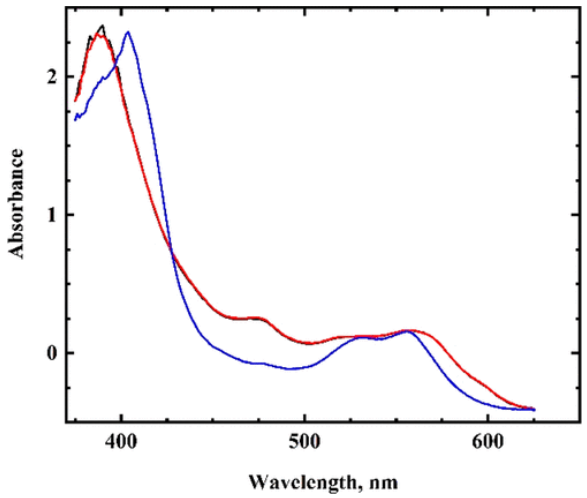

Figure 5. Stopped-flow spectra for the reaction of 0.6 mM $Fe(OEP)(NO)^-$ with 10 mM phenol in THF. Time: 1.0 ms (red), 1.0 s (black), and 1.0 ms with about 20% excess of potassium anthracenide reductant (blue).

Because of the small differences in the visible spectra of Fe(OEP)(NO) and Fe(OEP)(HNO) (and its hydrogen-bonded complex), additional experiments were carried out to verify that the species that were observed were at the $\{Fe(NO)\}^8$ oxidation state. When a solution containing 1 equiv of Fe(OEP)(NO) and 1 equiv of reducing agent was mixed with 10 mM phenol (Figure 5, black/red traces), a spectrum similar to Figure 4 was obtained. When there was a small excess (about 20%) of the reducing agent compared to Fe(OEP)(NO), a new band at 403 nm was immediately observed (Figure 5, blue trace). This species has been previously attributed to the reduction product of Fe(OEP)(HNO), $Fe(OEP)(NH_2OH)$.(32) The fact that the initial product can be further reduced confirms that the spectral species was at the $\{Fe(NO)\}^8$ oxidation level. The ^1H NMR, visible, and stopped-flow experiments are consistent with the following equilibrium:

$$Fe(OEP)(HNO) + PhO^- \rightleftarrows Fe(OEP)(NO)^- \cdots HOPh \quad (7)$$

The visible, voltammetric, and ^1H NMR data all show that the addition of phenol does not change the oxidation state of the $\{Fe(NO)\}^8$ species. The shift in the proton in the HNO moiety is consistent with reaction 7.

Resonance Raman Spectroscopy

Because of the challenges of infrared spectroscopy in identifying the $\{Fe(HNO)\}^8$ species, a series of experiments were carried out using resonance Raman spectroscopy. The room-temperature spectra were difficult to obtain because of the photo-oxidation of $Fe(OEP)(NO)^-$, even though the power was kept low. At 77 K, the ν_{NO} for $Fe(OEP)(NO)^-$ was consistent with the infrared data. In the low-frequency region, the ν_{FeNO} band was observed at 543 cm^{-1} (528 cm^{-1} for ^{15}N). This compares with 549 cm^{-1} for $Fe(TPP)(NO)^-$.(22) With the addition of 3,5-dcp, the ν_{FeNO} band at 543 cm^{-1} disappeared (Figure 6). The ν_{FeNO} for the product could be clearly seen only for the ^{15}N-complex at 638 cm^{-1}. This compares with the 628 cm^{-1} band for $Fe(H^{15}NO)$-myoglobin.(33) The difference spectrum (Figure 6, black trace) showed a peak at 666 cm^{-1} for the ^{14}N complex. The resonance Raman spectra in the high-frequency region showed no evidence of $Fe(OEP)(^{14}NO)$/$Fe(OEP)(^{15}NO)$, which would have been formed by the photo-oxidation of the $\{Fe(HNO)\}^8$ complex.

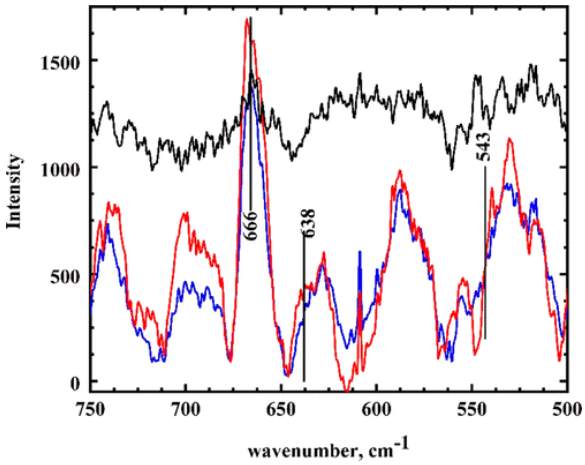

Figure 6. Resonance Raman spectra of 8 mM $Fe(OEP)(NO)^-$ in 3,5-dcp at 77 K. $Fe(OEP)(^{14}NO)^-$ + acid (blue), $Fe(OEP)(^{15}NO)^-$ + acid (red), and difference spectra (black).

DFT Calculations

In order to confirm these assignments, DFT calculations were carried out on an array of possible {Fe(NO)}^{8} species interacting with phenol. The ^{1}H NMR spectra of possible products (Figure 7) for the reaction of the Fe(OEP)(NO)$^-$ with phenolic species are shown in Table1. The structures studied were the hydrogen-bonded complexes between phenol and Fe(OEP)(NO)$^-$ via a N–H bond (1) or an O–H bond (5), Fe(OEP)(HNO) (2), several Fe(OEP)(HNO) complexes where phenolate (4) or phenol (3) can hydrogen bond to the HNO moiety, or a six coordinate Fe(OEP)(HNO) complex phenol (7). The final complex is the six coordinate Fe(OEP)(NO)(PhOH)$^-$ complex (6). The lack of resonances upfield from TMS excludes 6 and 7. In addition, the calculated proton HNO resonance for 7 is considerably downfield from the experimental value, and the shifts of the *meso* resonances are much larger than the observed values. The experimental chemical shift values for the HNO proton at 12.60 ppm agrees well with the calculated values of 12.24 ppm for 2, 13.51 ppm for 3, and 13.56 ppm for 4. The *meso*-protons are very sensitive to the Fe-displacement from the porphyrin plane, and the differences between the experimental and DFT-calculated values may be due to a somewhat stronger calculated Fe–N(porphyrin) bond. The hydrogen-bonded Fe(OEP)(HNO) complexes (2–4) are consistent with the data for the HNO resonance.

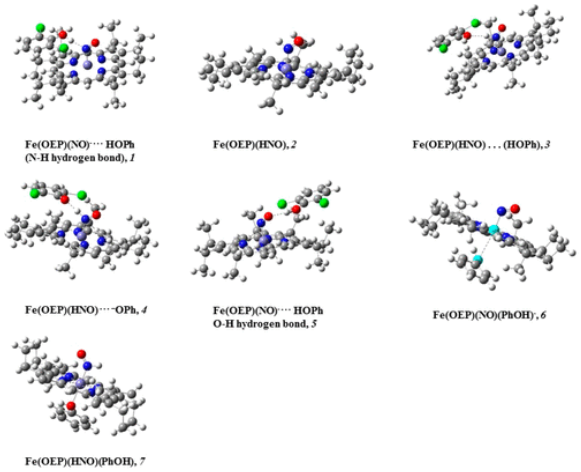

Figure 7. Structures for the complexes reported in Table1.

Table 1. DFT Calculations for the ^{1}H NMR Spectra of {Fe(OEP)(NO)}^{8} Species Using *Gaussian 09*

complex	δ_{HNO} (ppm)	δ_{HOPh} (ppm)	δ_{meso} (ppm)	functional
Fe(OEP)(NO)$^-$	**—**	**—**	**6.98, 7.01, 7.73, 7.83**	**m06L**
Fe(OEP)(NO)$^-$/HOPh, H-bond to N, 1	**–**	**6.06**	**7.65, 7.68, 7.84, 8.03**	**m06**
Fe(OEP)(HNO), 2	**12.24**	**—**	**9.92, 9.94, 10.11, 10.26**	**m06**
Fe(OEP)(HNO)/PhOH, 3	**13.51**	**3.17**	**8.89, 9.62, 9.74, 10.04**	**m06L**
Fe(OEP)(HNO)/PhO$^-$, 4	**13.56**	**—**	**8.93, 8.97, 9.14, 9.51**	**m06L**
Fe(OEP)(NO)$^-$/HOPh, H-bond to O, 5	**—**	**7.01**	**7.25, 7.71, 8.35, 8.46**	**m06L**
Fe(OEP)(NO)(PhOH)$^-$, 6	**—**	**–2.14**	**6.25, 6.99, 10.81, 12.18**	**m06**
Fe(OEP)(HNO)(PhOH), 7	**23.93**	**–7.03**	**9.67, 10.50, 10.70, 11.13**	**m06**

Structure 4, a Fe(OEP)(HNO) hydrogen-bonded phenolate complex, is unlikely considering previous kinetic studies. RRDE data(31) showed a first-order dependence of the observed rate of Fe(OEP)(HNO) on the concentration of phenolate. If the phenolate hydrogen-bonded species was significant in solution, the reaction should be zero-order. Overall analysis of the data shows that structure 2 or 3 is consistent with the protonated complex and structure 1 with the hydrogen-bonded complex. Both structures for the protonated complex show

a small upfield shift in the *meso*-protons. One could distinguish between 2 and 3 based on the 3.17 ppm resonance for the phenol proton, but fast exchange with free phenol may make this resonance hard to see. Both these species are 5-coordinate complexes, and hydrogen bonding with the HNO moiety is reasonable in THF. There is no evidence in either direction for the identity of the species. The effect of phenol on the equilibrium will depend upon whether one or both $\{Fe(NO)\}^8$ species are hydrogen-bonded.

The fact that DFT calculations iterated to either the HNO or NO^- hydrogen-bonded complex, depending upon the initial structure, indicates that there are two potential energy wells in the phenol-$\{Fe(NO)\}^8$ interaction (hydrogen-bonded or protonated). The position of equilibrium will depend upon solvation issues. The combination of the spectroscopic results and DFT calculation support the equilibrium described in reaction 7. We can obtain a rough estimate of the value of K from the data in Table S1 and estimated values for δ_{NO} and δ_{HNO} based on the DFT calculations. With the limited data, there is considerable uncertainty in the value. It does indicate though that the formation of Fe(OEP)(HNO) depends upon the temperature and the presence of other bases in proximity to the Fe-HNO moiety.

In addition to the ^{1}H NMR spectra, the vibrational spectra of the most probable species were also carried out (Table2). As was discussed in previous publications,(6,38) DFT calculations predicted higher energies for the ν_{NO} bands than the experimental value (1440 cm^{-1}).(38) When $Fe(OEP)(NO)^-$ is protonated, all the functionals predict a decrease in energy on the order of 48–86 cm^{-1}. Because the DFT values for the ν_{NO} bands of the anion are too high, the downshift might not occur as all the Fe(OEP)(HNO) values from DFT are above the experimental value for $Fe(OEP)(NO)^-$. Hydrogen bonding to Fe(OEP)(HNO) (species 3) leads to a small (3 cm^{-1}) downshift, while the formation of species 1 predicts a 29 cm^{-1} downshift. In the low-frequency region, the ν_{FeNO} band upshifts with the formation of the $\{Fe(NO)\}^8$ species. Formation of the Fe(OEP)(HNO) species (2) leads to a further upshift to the 641–675 cm^{-1} region depending upon the functional. These results are consistent with the resonance Raman spectra of Immoos et al.(17) and Czarnecki and Kincaid.(33) Hydrogen bonding of Fe(OEP)(HNO) with phenol (species 3) causes a small upshift (3 cm^{-1}), while hydrogen bonding with $Fe(OEP)(NO)^-$ (species 1) gives a band quite similar to species 2 (650 cm^{-1} for 1; 662 cm^{-1} for 2) but significantly upshifted from $Fe(OEP)(NO)^-$ (583 cm^{-1}). Given the uncertainty in the DFT values, it would be difficult to distinguish species 1–3 based on DFT calculations. The experimental resonance Raman spectra are consistent with the ^{1}H NMR results. However, it is not possible to unambiguously distinguish between the $\{Fe(HNO)\}^8$ and the hydrogen-bonded $\{Fe(NO)\}^8$ complexes based on vibrational spectroscopy because of the similarity of the vibrational bands. Further work is being undertaken to obtain resonance Raman spectra at room temperature, which would make it possible to determine the experimental values for $\{Fe(HNO)\}^8$.

Table 2. DFT Calculations for the Infrared Spectra of $\{Fe(NO)\}^8$ Species Using *Gaussian 09*

species	method	ν_{NO} (cm^{-1})	ν_{FeNO} (cm^{-1})	reference
$Fe(OEP)(NO)^-$	**bp86**	**1527**	**566**	**(6), this work**
	m06l	**1599**	**583**	**(6), this work**
	mpwvwn	**1483**	**546**	**(6), this work**
$Fe(OEP)(NO)^-$··· HOPh, 1	**m06l**	**1570**	**650**	**this work**
Fe(OEP)(HNO), 2	**bp86**	**1455**	**675**	**this work**
	m06l	**1599**	**583**	**this work**
	mpwvwn	**1397**	**641**	**this work**
Fe(OEP)(HNO)···HOPh, 3	**m06l**	**1548**	**665**	**this work**

The importance of hydrogen bonds in stabilizing the HNO moiety in myoglobin has been studied by Sulc et al.(16) Their ^{1}H NMR studies showed that hydrogen bonding occurred between the oxygen atom of the HNO group and His64. Yang et al.(39) carried out additional DFT calculations on models of myoglobin-HNO including

hydrogen bonding to water, as well as hydrogen bonding between His64 and the hydrogen of the HNO moiety. The addition of the hydrogen bonding to water at either the H–N group or the terminal oxygen (with rotation of the HNO group) provided additional stabilization and a qualitative improvement in the spectroscopic properties. The ability of water and/or His64 to hydrogen bond to the {Fe(NO)}^{8} moiety should lead to visible and vibrational spectroscopic properties similar to {Fe(HNO)}^{8} species.

Many spectroscopic techniques are carried out at 77 K, and care must be taken to ensure that the room-temperature and low-temperature species are identical. This equilibrium may explain recent voltammetric and spectroscopic data for the reaction of Fe(TPP)(NO)$^-$ with a protic room-temperature ionic liquid (RTIL).(40) Room-temperature voltammetric data indicated the formation of the Fe(TPP)(HNO) complex, while resonance Raman data at 77 K showed no shift in the low-frequency band of the Fe-HNO band from the Fe-NO$^-$ band at 553 cm^{-1}. Other spectroscopic evidence showed that the iron-nitrosyl group was reduced in the presence and absence of the protic RTIL. This result may be explained by the shift in the protonation/hydrogen bonding equilibrium in going from room temperature to 77 K, where the hydrogen-bonded complex was formed. Further research is being carried out to verify this.

Conclusions

The equilibrium between the protonation of Fe(OEP)(NO)$^-$ and the hydrogen-bonded complex can be shifted as a function of temperature. This shift has precedence in the literature, as was discussed in the Introduction.(28−30) This equilibrium will complicate the isolation of the Fe(OEP)(HNO) complex when Brønsted bases are present. In enzymes, the presence of basic amino acids may affect the stability of the {Fe(NO)}^{8} species at low temperatures. In this work, low temperatures favored the hydrogen-bonded complex over protonation, but there is no guarantee that will always be the case. Because many spectroscopic techniques are carried out at 77 K, care must be taken to ensure that the room-temperature and low-temperature species are identical.

The visible spectra for {Fe(NO)}^{8} species are quite sensitive to the solvation environment, especially in the presence of hydrogen-bonding species. Hydrogen bonding and the presence of water molecules are common in many protein environments including myoglobin. This work shows that the visible spectra of the hydrogen-bonded {Fe(NO)}^{8} and {Fe(HNO)}^{8} complexes are quite similar and are distinct from the {Fe(NO)}^{8} complex without hydrogen bonding. While there are some differences in the vibrational spectra, the hydrogen-bonded {Fe(NO)}^{8} and {Fe(HNO)}^{8} complexes are more similar to each other than to {Fe(NO)}^{8} without hydrogen bonding. Other spectroscopic techniques such as ^{1}H NMR spectra should be used to confirm the assignment.

Supporting Information

The Supporting Information is available free of charge on the ACS Publications website at DOI: 10.1021/acs.inorgchem.9b01447.

Chemical shift for HNO resonance and *K* value as calculated from eq 4 as a function of temperature; ^{2}H NMR spectrum of Fe(OEP)(NO)$^-$ with 3,5-dichlorophenol-d_4 in THF at −40 °C; rotating ring disk voltammetry of Fe(OEP)(NO) with and without phenol; stopped-flow spectra of Fe(OEP)(NO)$^-$ reaction with 2,6-dichlorophenol in THF (PDF)

Original data and checkpoint files for DFT calculations (.fchk, .opju, .ppt, .xslx files) can be found at: https://https://epublications.marquette.edu/chem_data/3/

pdf

ic9b01447_si_001.pdf (340.04 kb)

The authors declare no competing financial interest.

Terms & Conditions

References

1 Speelman, A. L.; Lehnert, N. Heme versus Non-Heme Iron-Nitroxyl {FeN(H)O}^{8} Complexes: Electronic Structure and Biologically Relevant Reactivity. *Acc. Chem. Res.* **2014**, *47* (4), 1106– 1116, DOI: 10.1021/ar400256u

2 Abucayon, E. G.; Khade, R. L.; Powell, D. R.; Zhang, Y.; Richter-Addo, G. B. Hydride Attack on a Coordinated Ferric Nitrosyl: Experimental and DFT Evidence for the Formation of a Heme Model-HNO Derivative. *J. Am. Chem. Soc.* **2016**, *138* (1), 104– 107, DOI: 10.1021/jacs.5b12008

3 Khade, R. L.; Yang, Y.; Shi, Y.; Zhang, Y. HNO-binding in heme proteins: Effects of iron oxidation state, axial ligand, and protein environment. *Angew. Chem., Int. Ed.* **2016**, *55* (48), 15058– 15061, DOI: 10.1002/anie.201608539

4 Bianco, C. L.; Toscano, J. P.; Bartberger, M. D.; Fukuto, J. M. The chemical biology of HNO signaling. *Arch. Biochem. Biophys.* **2017**, *617*, 129– 136, DOI: 10.1016/j.abb.2016.08.014

5 Confer, A. M.; McQuilken, A. C.; Matsumura, H.; Moënne-Loccoz, P.; Goldberg, D. P. A Nonheme, High-Spin {FeNO}^{8} Complex that Spontaneously Generates N_2O. *J. Am. Chem. Soc.* **2017**, *139* (31), 10621– 10624, DOI: 10.1021/jacs.7b05549

6 Rahman, M. H.; Ryan, M. D. Redox and Spectroscopic Properties of Iron Porphyrin Nitroxyl in the Presence of Weak Acids. *Inorg. Chem.* **2017**, *56* (6), 3302– 3309, DOI: 10.1021/acs.inorgchem.6b02665

7 Zhang, K.; Thynell, S. T. Examination of the Mechanism of the Yield of N_2O from Nitroxyl (HNO) in the Solution Phase by Theoretical Calculations. *J. Phys. Chem. A* **2017**, *121* (23), 4505– 4516, DOI: 10.1021/acs.jpca.7b01152

8 Einsle, O.; Messerschmidt, A.; Huber, R.; Kroneck, P. M. H.; Neese, F. Mechanism of the Six-Electron Reduction of Nitrite to Ammonia by Cytochrome *c* Nitrite Reductase. *J. Am. Chem. Soc.* **2002**, *124* (39), 11737– 11745, DOI: 10.1021/ja0206487

9 Bykov, D.; Neese, F. Six-Electron Reduction of Nitrite to Ammonia by Cytochrome *c* Nitrite Reductase: Insights from Density Functional Theory Studies. *Inorg. Chem.* **2015**, *54* (19), 9303– 9316, DOI: 10.1021/acs.inorgchem.5b01506

10 Daiber, A.; Shoun, H.; Ullrich, V. Nitric oxide reductase ($P450_{nor}$) from *Fusarium oxysporum*. *J. Inorg. Biochem.* **2005**, *99* (1), 185– 193, DOI: 10.1016/j.jinorgbio.2004.09.018

11 Averill, B. A. Dissimilatory nitrite and nitric oxide reductases. *Chem. Rev.* **1996**, *96* (7), 2951– 2964, DOI: 10.1021/cr950056p

12 Cabail, M. Z.; Kostera, J.; Pacheco, A. A. Laser Photoinitiated Nitrosylation of 3-Electron Reduced Nm europaea Hydroxylamine Oxidoreductase: Kinetic and Thermodynamic Properties of the Nitrosylated Enzyme. *Inorg. Chem.* **2005**, *44* (2), 225– 231, DOI: 10.1021/ic048822a

13 Paolocci, N.; Jackson, M. I.; Lopez, B. E.; Miranda, K.; Tocchetti, C. G.; Wink, D. A.; Hobbs, A. J.; Fukuto, J. M. The pharmacology of nitroxyl (HNO) and its therapeutic potential: Not just the janus face of NO. *Pharmacol. Ther.* **2007**, *113* (2), 442– 458, DOI: 10.1016/j.pharmthera.2006.11.002

14 Miranda, K. M. The chemistry of nitroxyl (HNO) and implications in biology. *Coord. Chem. Rev.* **2005**, *249* (3–4), 433– 455, DOI: 10.1016/j.ccr.2004.08.010
15 Lin, R.; Farmer, P. J. The HNO Adduct of Myoglobin: Synthesis and Characterization. *J. Am. Chem. Soc.* **2000**, *122* (10), 2393– 2394, DOI: 10.1021/ja994079n
16 Sulc, F.; Fleischer, E.; Farmer, P. J.; Ma, D. J.; La Mar, G. N. ^{1}H NMR structure of the heme pocket of HNO-myoglobin. *JBIC, J. Biol. Inorg. Chem.* **2003**, *8* (3), 348– 352, DOI: 10.1007/s00775-002-0422-7
17 Immoos, C. E.; Sulc, F.; Farmer, P. J.; Czarnecki, K.; Bocian, D. F.; Levina, A.; Aitken, J. B.; Armstrong, R. S.; Lay, P. A. Bonding in HNO-Myoglobin as Characterized by X-ray Absorption and Resonance Raman Spectroscopies. *J. Am. Chem. Soc.* **2005**, *127* (3), 814– 815, DOI: 10.1021/ja0433727
18 Kumar, M. R.; Pervitsky, D.; Chen, L.; Poulos, T. L.; Kundu, S.; Hargrove, M. S.; Rivera, E. J.; Diaz, A. D.; Colón, J. L.; Farmer, P. J. Nitrosyl hydride (HNO) as an O_2 analogue: long-lived HNO-adducts of ferrous globins. *Biochemistry* **2009**, *48* (22), 5018– 5025, DOI: 10.1021/bi900122r
19 Farmer, P. J.; Sulc, F. Coordination chemistry of the HNO ligand with hemes and synthetic coordination complexes. *J. Inorg. Biochem.* **2005**, *99* (1), 166– 184, DOI: 10.1016/j.jinorgbio.2004.11.005
20 Abucayon, E. G.; Khade, R. L.; Powell, D. R.; Shaw, M. J.; Zhang, Y.; Richter-Addo, G. B. Over or under: hydride attack at the metal versus the coordinated nitrosyl ligand in ferric nitrosyl porphyrins. *Dalton Trans* **2016**, *45* (45), 18259– 18266, DOI: 10.1039/C6DT03860C
21 Gao, Y.; Toubaei, A.; Kong, X.; Wu, G. Acidity and Hydrogen Exchange Dynamics of Iron(II)-Bound Nitroxyl in Aqueous Solution. *Angew. Chem., Int. Ed.* **2014**, *53* (43), 11547– 11551, DOI: 10.1002/anie.201407018
22 Choi, I.-K.; Liu, Y.; Feng, D.; Paeng, K. J.; Ryan, M. D. Electrochemical and spectroscopic studies of iron porphyrin nitrosyls and their reduction products. *Inorg. Chem.* **1991**, *30* (8), 1832– 1839, DOI: 10.1021/ic00008a028
23 Goodrich, L. E.; Roy, S.; Alp, E. E.; Zhao, J.; Hu, M. Y.; Lehnert, N. Electronic Structure and Biologically Relevant Reactivity of Low-Spin {FeNO}^{8} Porphyrin Model Complexes: New Insight from a Bis-Picket Fence Porphyrin. *Inorg. Chem.* **2013**, *52* (13), 7766– 7780, DOI: 10.1021/ic400977h
24 Levin, N.; Codesido, N. O.; Marcolongo, J. P.; Alborés, P.; Weyhermüller, T.; Olabe, J. A.; Slep, L. D. Remarkable Changes of the Acidity of Bound Nitroxyl (HNO) in the $[Ru(Me_3[9]aneN_3)(L^2)(NO)]^{n+}$ Family (n = 1–3). Systematic Structural and Chemical Exploration and Bioinorganic Chemistry Implications. *Inorg. Chem.* **2018**, *57* (19), 12270– 12281, DOI: 10.1021/acs.inorgchem.8b01958
25 Ling, Y.; Mills, C.; Weber, R.; Yang, L.; Zhang, Y. NMR, IR/Raman, and Structural Properties in HNO and RNO (R = Alkyl and Aryl) Metalloporphyrins with Implication for the HNO-Myoglobin Complex. *J. Am. Chem. Soc.* **2010**, *132* (5), 1583– 1591, DOI: 10.1021/ja907342s
26 Zhang, Y. Computational investigations of HNO in biology. *J. Inorg. Biochem.* **2013**, *118*, 191– 200, DOI: 10.1016/j.jinorgbio.2012.09.023
27 Denisov, G. S.; Golubev, N. S. Localization and moving of a proton inside hydrogen-bonded complexes in aprotic solvents. *J. Mol. Struct.* **1981**, *75* (2), 311– 326, DOI: 10.1016/0022-2860(81)85245-3
28 Zundel, G. Proton transfer in and proton polarizability of hydrogen bonds: IR and theoretical studies regarding mechanisms in biological systems. *J. Mol. Struct.* **1988**, *177*, 43– 68, DOI: 10.1016/0022-2860(88)80078-4
29 Golubev, N. S.; Denisov, G. S.; Kol'tsov, A. I. Study of systems with reversible proton transition in complexes with hydrogen bonds by proton NMR spectroscopy at low temperatures. *Proc. USSR Acad. Sci.* **1977**, *232* (4), 144– 147
30 Golubev, N. S.; Smirnov, S. N.; Tolstoy, P. M.; Sharif, S.; Toney, M. D.; Denisov, G. S.; Limbach, H. H. Observation by NMR of the tautomerism of an intramolecular OHOHN-charge relay chain in a model Schiff base. *J. Mol. Struct.* **2007**, *844–845*, 319– 327, DOI: 10.1016/j.molstruc.2007.04.015
31 Rahman, M. H.; Ryan, M. D. The Use of RRDE Voltammetry to Study Acid-Base Reactions in Unbuffered Solutions. *Electrochim. Acta* **2018**, *281*, 17– 23, DOI: 10.1016/j.electacta.2018.05.125

32 Rahman, M. H.; Ryan, M. D. Insight into Solvent Coordination of An Iron Porphyrin Hydroxylamine Complex from ^{1}H NMR, FTIR and DFT Evidence. *Eur. J. Inorg. Chem.* **2018**, *2018* (16), 1762– 1765, DOI: 10.1002/ejic.201800040

33 Czarnecki, K.; Kincaid, J. R. Effective methods for preparation and characterization of HNO-adducts of heme proteins. *J. Raman Spectrosc.* **2012**, *43* (9), 1343– 1345, DOI: 10.1002/jrs.4046

34 Kundakarla, N.; Lindeman, S.; Rahman, M. H.; Ryan, M. D. X-ray Structure and Properties of the Ferrous Octaethylporphyrin Nitroxyl Complex. *Inorg. Chem.* **2016**, *55* (5), 2070– 5, DOI: 10.1021/acs.inorgchem.5b02384

35 Choi, I.-K.; Liu, Y. M.; Wei, Z.; Ryan, M. D. Reactions of hydroxylamine with metal porphyrins. *Inorg. Chem.* **1997**, *36* (14), 3113– 3118, DOI: 10.1021/ic9605783

36 Liu, Y. M.; DeSilva, C.; Ryan, M. D. Electrochemistry of nitrite reductase model compounds. 6. Voltammetric and spectroelectrochemical studies of iron(II) nitrosyl complexes with porphyrins, hydroporphyrins and porphinones. *Inorg. Chim. Acta* **1997**, *258* (2), 247– 255, DOI: 10.1016/S0020-1693(96)05547-8

37 Ovchinnikov, I. M.; Ksenofontov, V. A. Effect of physicochemical processes on the isotopic analysis of nitrogen by the NMR spin-spin splitting method. *J. Appl. Spectrosc.* **1976**, *24* (5), 636– 639, DOI: 10.1007/BF00633445

38 Wei, Z.; Ryan, M. D. Infrared Spectroelectrochemical Reduction of Iron Porphyrin Complexes. *Inorg. Chem.* **2010**, *49* (15), 6948– 6954, DOI: 10.1021/ic100614h

39 Yang, L.; Ling, Y.; Zhang, Y. HNO Binding in a Heme Protein: Structures, Spectroscopic Properties, and Stabilities. *J. Am. Chem. Soc.* **2011**, *133* (35), 13814– 13817, DOI: 10.1021/ja204072j

40 Atifi, A.; Mak, P. J.; Ryan, M. D. Proton-coupled reduction of an iron nitrosyl porphyrin in the protic ionic liquid nanodomain. *Electrochim. Acta* **2019**, *295*, 735– 741, DOI: 10.1016/j.electacta.2018.10.179